Int. J. Multiphase Flow Vol. 15, No. 3, pp. 341–356, 1989
Printed in Great Britain.

0301-9322/89 $3.00 + 0.00

BEHAVIOR OF DISTURBANCE WAVES UNDER HYDRODYNAMIC NON-EQUILIBRIUM CONDITIONS

T. SAWAI and S. YAMAUCHI
Department of Mechanical Engineering, Takamatsu National College of Technology, 355 Chokushi-cho, Takamatsu 761, Japan

S. NAKANISHI
Department of Chemical Engineering, Himeji Institute of Technology, 2167 Shosha, Himeji 671-22, Japan

(*Received* 1 *October* 1988; *in revised form* 15 *November* 1988)

Abstract—The behavior of disturbance waves in boiling steam–water two-phase flow is experimentally investigated at a pressure of 2.95 MPa. A new type of hydrodynamic non-equilibrium is introduced: the imbalance in the liquid distribution between the base film and individual disturbance waves ("B–D non-equilibrium"). This non-equilibrium is postulated to be one of the main causes of the difference between the behavior of disturbance waves in a boiling system and that in the corresponding adiabatic air–water system, and is confirmed by examination of its recovery process in unheated channels attached downstream of a boiling section and by its simulation in air–water shear flow. Finally, examination of the data for fully-developed adiabatic flow suggests some difference in the behavior of disturbance waves in the steam–water system and in the air–water system.

Key Words: multiphase flow, boiling flow, disturbance wave, hydrodynamic non-equilibrium

1. INTRODUCTION

The notion of hydrodynamic non-equilibrium in boiling two-phase flow was proposed to explain the mechanism of dryout and to predict it by the Harwell group (Tong & Hewitt 1972); heat transfer and dryout are strongly dependent on the degree of departure from the fully-developed adiabatic system in the liquid flow distribution between film and entrainment. Meanwhile, it is well-known that the role of the disturbance wave is not insignificant in the annular flow regime, even in boiling flow. So it is worthwhile investigating behavior of the disturbance wave under hydrodynamic non-equilibrium conditions. However, almost all experimental works on the disturbance wave have been conducted with adiabatic air–water systems in the neighborhood of atmospheric pressure. One exception is the work by Brown *et al.* (1975), who reported the hydrodynamic non-equilibrium effects on the disturbance wave under relatively low quality and low pressure conditions. The other is our previous work (Nakanishi *et al.* 1985), in which the behavior of the disturbance wave in the dryout region was experimentally investigated with a boiling steam–water system at a pressure of 2.95 MPa and compared with that in the corresponding adiabatic air–water system. The observed difference between the results with the two systems suggested the existence of a new type of hydrodynamic non-equilibrium, i.e. an imbalance in the liquid distribution between the base film and individual disturbance waves. Hereafter, this type of hydrodynamic non-equilibrium is referred to as the "B–D non-equilibrium" and the one between the entrainment and the liquid film as the "E–F non-equilibrium". Introduction of the B–D non-equilibrium threw light on the behavior of the disturbance wave in boiling two-phase flow.

In the present study, new experimental data on disturbance waves with a boiling steam–water vertical upwards system were accumulated for a wider range of quality >0.5. In order to confirm the notion of the B–D non-equilibrium, which was postulated to be one of the main causes of the difference between the behavior of disturbance waves in a boiling system and that in the corresponding adiabatic air–water system, the recovery process of hydrodynamic equilibrium was experimentally investigated in an unheated channel with steam–water flow. Furthermore, through a simulation of the B–D non-equilibrium with air–water shear flow, it was observed how the fully-developed film flow was established by measuring variations in the disturbance wave and base

film along the channel. Finally, in connection with identifying the cause of the observed difference in the behavior of disturbance waves between corresponding steam–water and air–water systems in fully-developed adiabatic flow, the effect of the gas–liquid density ratio was experimentally investigated in the air–water system and was found not to be the reason.

2. EXPERIMENTAL APPARATUS AND PROCEDURES

2.1. Steam–water system

Experiments with the steam–water system were conducted on the same test rig as used in our earlier CHF study (Nakanishi *et al.* 1982). The test sections were made of AISI-304 stainless steel tubes, 4 mm i.d. In the present study, two versions of the test sections were employed. Arrangement I (figure 1) was the same as that used in our previous work (Nakanishi *et al.* 1985) and was used for the acquisition of boiling flow data over a wide quality range (down to 0.5) which enriched our data accumulation. Arrangement II (figure 2) was newly made to obtain data on the recovery process of the hydrodynamic equilibrium due to boiling. Test section I was divided into two parts: the upstream heated section and the downstream unheated section. The former section was 800 mm long and was moved by sliding two movable bus-bars in accordance with the length of the unheated section, which was one of three values, 140, 452 and 848 mm; these lengths corresponded to the length-to-diameter ratio (L/D), 35, 113 and 212, respectively. Between test sections I and II, the conductance probe was inserted to measure the film thickness at the exit of the unheated section. Figure 3 shows the conductance probe block. The experimental conditions were as follows: system pressure, 2.95 MPa; mass flux, 300 and 500 kg/m^2 s; heat flux, 0.26–1.34 MW/m^2; quality at the inlet of the unheated section, >0.5.

The experimental procedure was as follows. Feed water was prepared to the specified subcooling temperature in the preheater section, which was dosed with KCl to enhance the electrical conductivity. A dose rate of 3.75 mg/kg H_2O was used for measurements in the quality range 0.5–0.8 and 1.25 mg/kg H_2O for quality >0.8. After the pressure, mass flux, inlet subcooling and heat flux

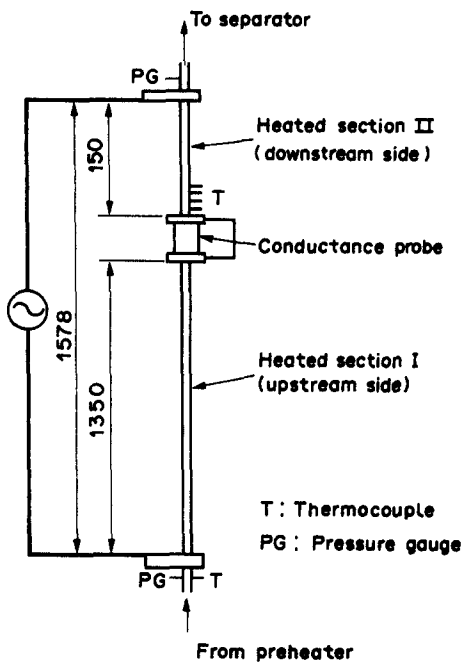

Figure 1. Test section for the steam–water system (arrangement I).

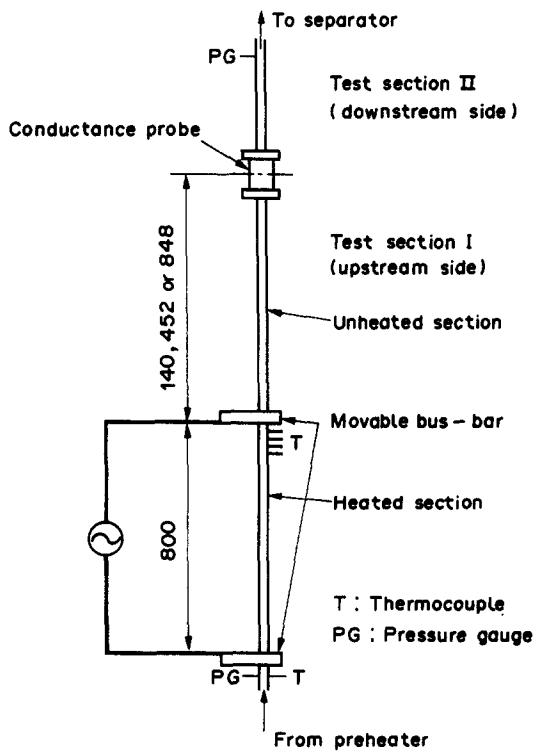

Figure 2. Test section for the steam–water system (arrangement II).

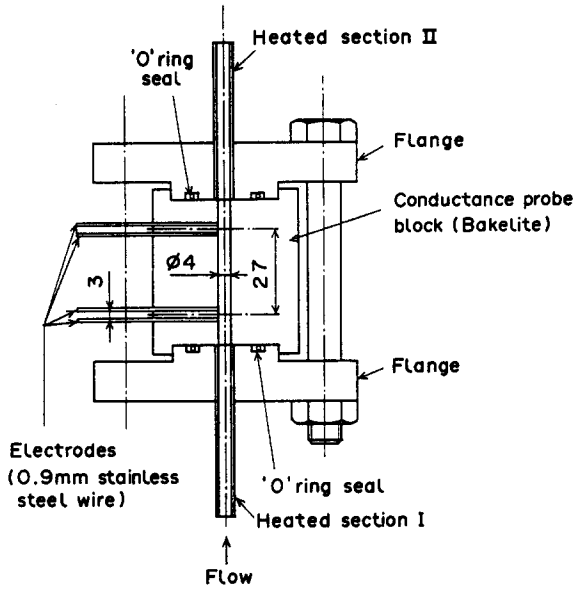

Figure 3. Conductance probe block.

had been maintained at the specified values for more than several minutes it was assumed that steady state was attained, and the output signals from the conductance probes and thermocouples were recorded; the latter were spot-welded on the outer surface of the heated section.

2.2. Air–water system

2.2.1. Tubular test channel. In order to investigate the difference between the steam–water and air–water systems in fully-developed adiabatic flow, a number of experiments were conducted with the adiabatic air–water system at three different values of the gas–liquid density ratio (ρ_L/ρ_G = 802, 276 and 152) which corresponded to the system pressure values of 103, 299 and 544 kPa, respectively. The test section consisted of a vertical acrylic tube of 5 mm i.d. The film thickness fluctuation was measured by conductance probes which were located 1.9 m downstream from the mixer. The superficial velocities of the air and water phases were set equal to those of steam and water in the corresponding boiling flow.

2.2.2. Rectangular test channel. To simulate the probable non-equilibrium state in the boiling flow under an annular flow regime, air–water two-phase shear flow was used. In this simulation, a horizontal flow was used because of the difficulty of the experiment with a vertical flow, although the gravitational force might influence the behavior of the disturbance wave. The test rig and the test section are shown in figures 4 and 5, respectively. Artificial non-equilibrium was realized by sucking part of the liquid film flow of fully-developed flow.

Air from a blower flows through a control damper and a metering orifice and then enters an inlet section. Water from the head tank also flows through a metering orifice and a needle valve and is introduced to the inlet section through a narrow slit positioned at the bottom side of the inlet section. The inlet section is sufficiently long to obtain fully-developed two-phase shear flow (3005 mm length) and is smoothly connected to a test section. At the latter inlet, part of the liquid film flow is sucked through the porous wall section along the bottom with the aid of a vacuum pump. The sucked liquid flow is measured with a rotameter and returned to a receiver. The shear flow from the test section is introduced into an air–water separator. The water separated therein is collected in a receiver and is then returned to the head tank with the aid of a gear pump.

The test section (200 mm width, 30 mm height, 2750 mm length) was made of acrylic resin and arranged horizontally. Twelve pairs of conductance probe electrodes (3 mm dia) were mounted 100–300 mm apart on the bottom plate as shown in figure 5, where the numerical figures 1–12 correspond to the number of the conductance probe. The electrodes in each pair of conductance probes were embedded 20 mm apart perpendicular to the flow direction. For measurement of the propagation velocity and the time separation of disturbance waves, wave whose height was greater

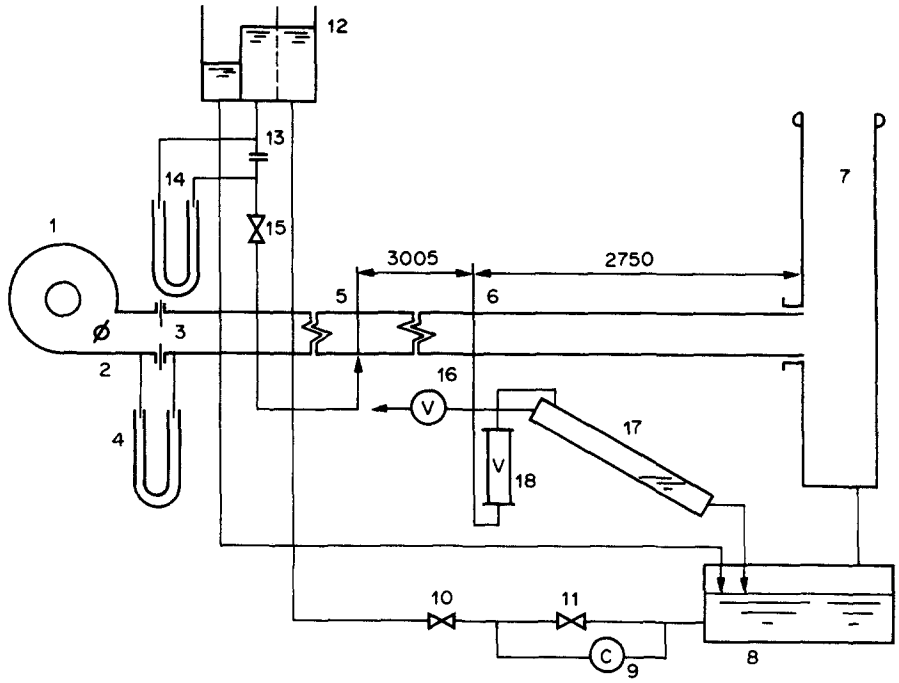

1 Blower
2 Control damper
3 Orifice
4 Manometer
5 Mixing device
6 Test section
7 Separator
8 Receiver
9 Pump
10 Needle valve
11 Needle valve
12 Head tank
13 Orifice
14 Manometer
15 Needle valve
16 Vacuum pump
17 Vacuum section
18 Rotameter

Figure 4. Flow diagram of the test rig for air–water shear flow.

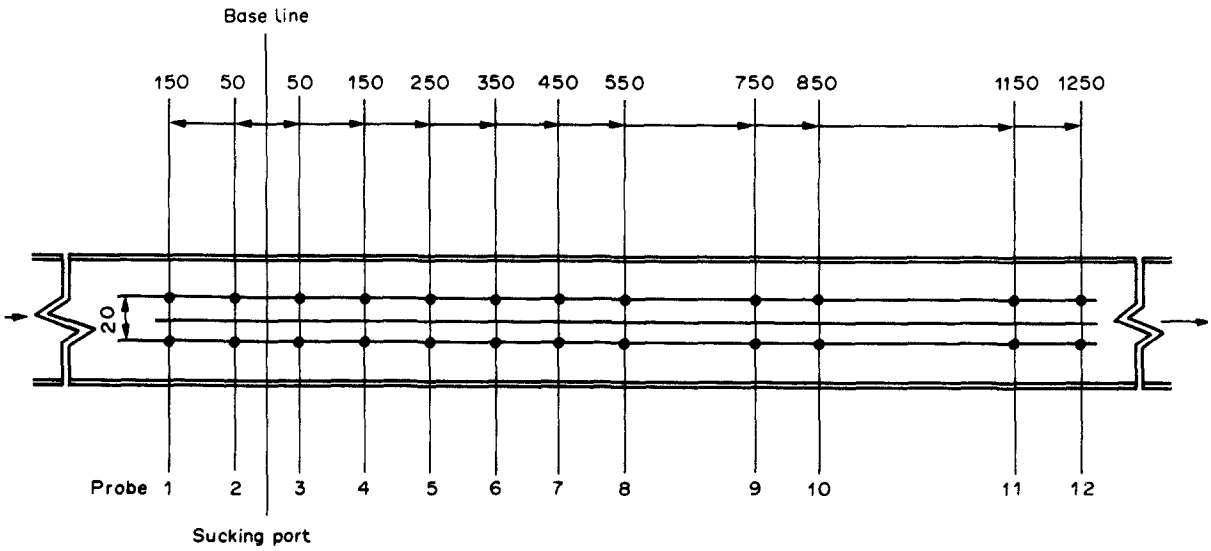

Figure 5. Test section for B–D non-equilibrium simulation.

than the sum of the base film thickness at each measuring point (h_b) and one-half of that before sucking, were counted as disturbance waves.

2.3. Data processing method

The output signal from the conductance probe was processed by the Laboratory Automation System at the Computation Center, Osaka University. The sampling frequency was chosen as 3 kHz for the steam–water system and 2 kHz for the air–water system. In order to eliminate "ripples" and noise components from the output signal, the Fourier transform smoothing method and the adaptive smoothing method of Kawata & Minami (1984) were applied to the data of the steam–water and air–water systems, respectively. The total sampling time was 10–20 s.

3. RESULTS AND DISCUSSION FOR THE STEAM–WATER SYSTEM

3.1. Liquid film thickness fluctuation

Figure 6 is a typical example of the film thickness fluctuation recorded just downstream of the exit of the heated section in a run with arrangement I (figure 1). The profile of peaks corresponding to the disturbance wave comprises a fairly steep front face and a long-tailed rear face, which is one of the notable features of a disturbance wave in boiling flow.

Figure 7 shows a set of film thickness recordings taken after the unheated section, for three different lengths ($L/D = 35$, 113 and 212), in arrangement II (figure 2); it should be noted that these three data sets were obtained on different runs. As disturbance waves advance along the unheated section, they lose the steepness of their front faces and finally, at $L/D = 212$, acquire a relatively gentler slope at both the front and rear, while the base film, which is easily distinguishable from the disturbance waves at the inlet zone of the unheated section, distorts at this point. Analogous situations were also observed for other run conditions.

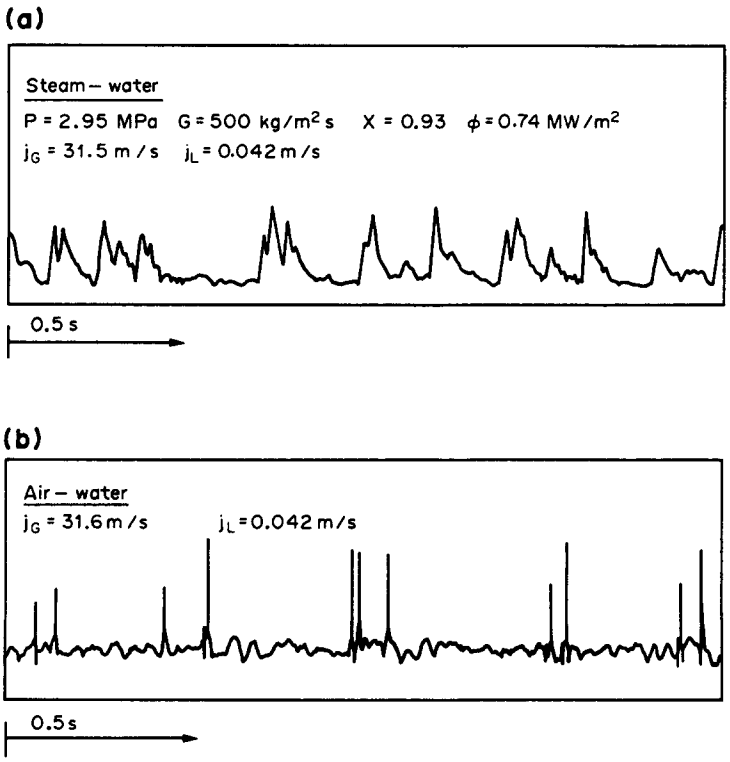

Figure 6. Recordings of the liquid film thickness signals: (a) boiling steam–water system; (b) adiabatic air–water system.

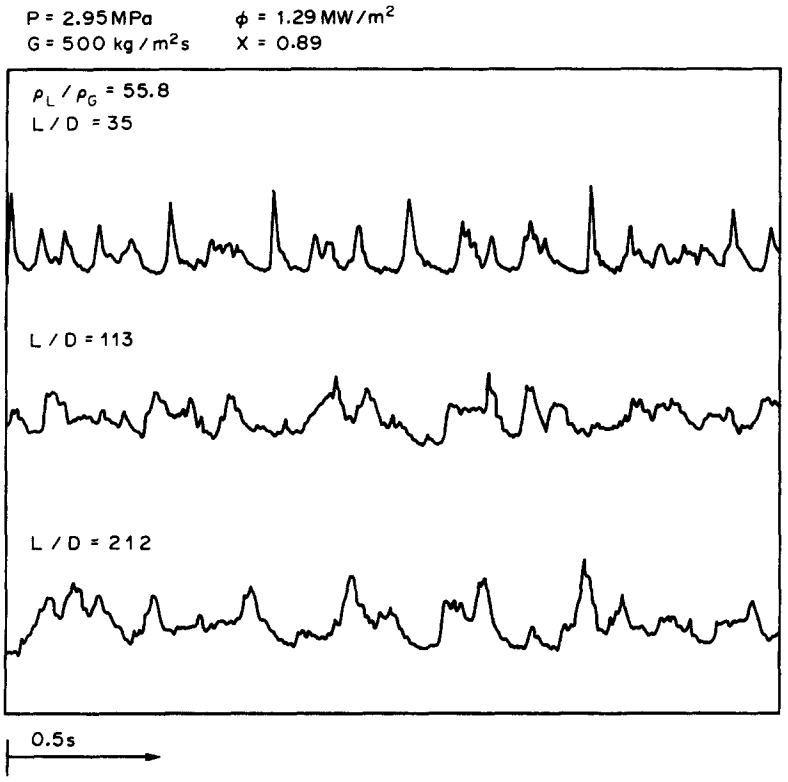

Figure 7. Variation of the film thickness fluctuation along the unheated section (steam–water system).

3.2. Time separation of the disturbance waves

The time separation of the disturbance waves was defined as the time elapsed between the passing of two successive disturbance waves observed at a fixed position. Figure 8 shows the variation in the mean time separation, $\bar{T}_d$, along the unheated channel for various inlet qualities. As can be seen, except for the data in the dryout quality region, it increases as L/D increases. This trend can be seen more clearly at higher mass flux values, $G = 500$ kg/m^2 s, and does not attain its asymptotic value even at the location of $L/D = 212$.

Figure 9 shows the mean time separation, $\bar{T}_d$, vs quality, X, for unheated sections of various lengths, L/D. The solid lines represent the data from the adiabatic air–water system with the corresponding gas and liquid superficial velocities obtained at three pressure levels. The effect of heat flux on the mean time separation was not significant under the present experimental conditions, so the values of heat flux for individual data are not shown in the figure. It is observed that the mean time separation in the boiling flow increases with quality much more slowly than in the unheated section with the steam–water system. This observational result cannot be interpreted only in terms of the E–F non-equilibrium. According to this concept, in the relatively high quality region, the film flow rate must be smaller than that at E–F equilibrium conditions and in turn the disturbance wave must attenuate more rapidly in the heated section than in the unheated section; so, a larger time separation must be observed in the former. However, the mean wave time separation is smaller in the heated section than in the unheated section. On the other hand, the B–D non-equilibrium is able to support the following interpretation of this phenomenon. In the high quality region in the boiling flow, the mass of the individual disturbance wave which travels over the base film is excessive compared with that in the B–D equilibrium condition, because of two reasons: (i) evaporation proceeds more intensely at the part of the base film not covered by the disturbance wave, which makes the thickness of the base film thinner in the boiling flow than in the corresponding adiabatic flow; and (ii) each body of the disturbance wave is transported from the upstream region which corresponds to smaller quality and, consequently, has excessive mass compared with that in the B–D equilibrium condition. If this non-equilibrium flow enters an unheated channel, each disturbance

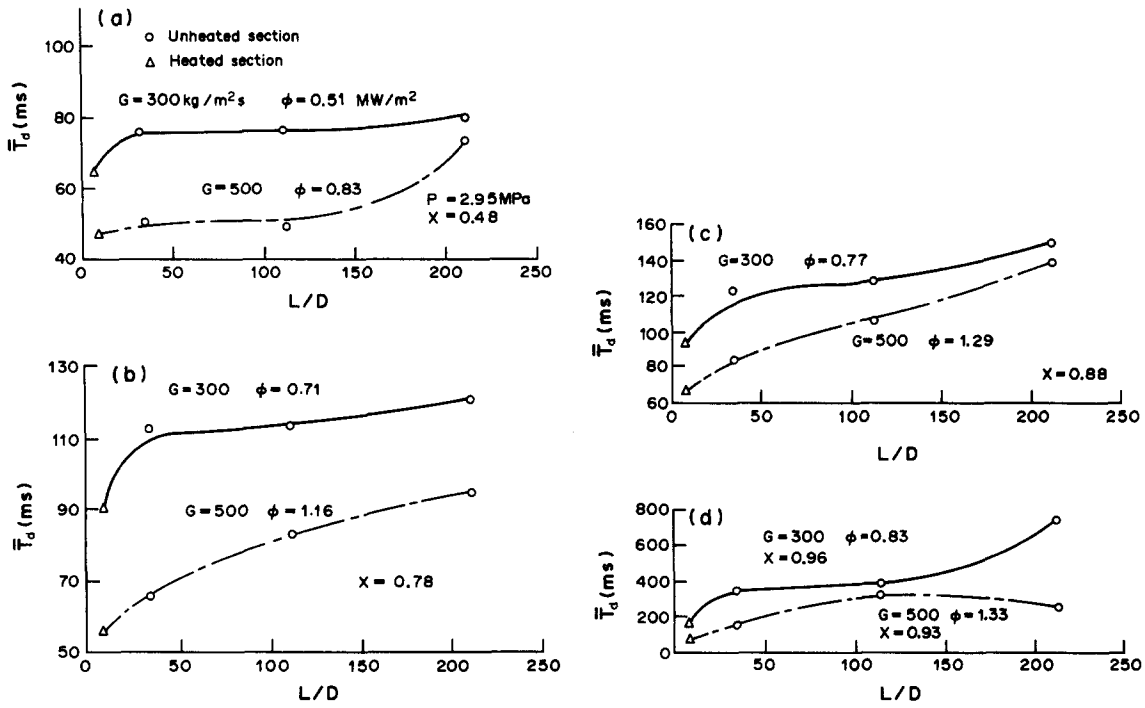

Figure 8. Variation of the time separation along the unheated channel (steam–water system).

wave in the non-equilibrium state advances along the channel, feeding its excess liquid to the base film and approaching the B–D hydrodynamic equilibrium state. In this process the disturbance wave attenuates and the wave time separation increases along the channel. This picture is also supported by the data on the wave profile (figure 7), in which the base film is already indistinguishable from the disturbance waves for $L/D = 212$. Even in the dryout region, the disturbance waves survive owing to the B–D non-equilibrium and thus induce temperature fluctuations whenever they arrive at the dryout front (Nakanishi *et al.* 1985).

Employment of a sufficiently long unheated section in the steam–water system realized a near B–D equilibrium, or fully-developed adiabatic flow, but resulted in somewhat different behavior of the disturbance waves from that in the air–water system. In order to clarify this difference in more detail, one of the possible causes, i.e. the difference in the gas–liquid density ratio, ρ_L/ρ_G, was examined. Although other physical properties such as surface tension, viscosity and so on, may have some effect it should be noted that the effect of the difference in gas density between the two systems is the greatest. As can be seen from figure 9, the gas–liquid density ratio data obtained with three different values of system pressure for the air–water system show a trend somewhat different from that in the unheated steam–water system, where $\rho_L/\rho_G = 55.8$. The fact that this discrepancy increases with the system pressure suggests that the difference between the above two systems appears to be due to something other than the effect of the gas–liquid density ratio. Further investigations are required to obtain definite conclusions.

3.3. Propagation velocity of the disturbance waves

Figure 10 represents the variation of the mean value, $\bar{U}_d$, of the propagation velocity of the disturbance waves in the unheated channel. For comparison, in figure 10(a), the data by Brown *et al.* (1975) for $G = 297$ kg/m² s, $X = 0.53$ and $P = 0.375$ MPa are also plotted. The discrepancy with our data might be attributable to the differences in system pressure and tube diameter. An important common feature is that the mean value of the propagation velocity is not affected by hydrodynamic non-equilibrium due to heating showing no significant change along the unheated channel. This is confirmed for other experimental conditions, under which the degree of hydrodynamic non-equilibrium was estimated to be greater, as shown in figures 10(b, c). The singular behavior of the

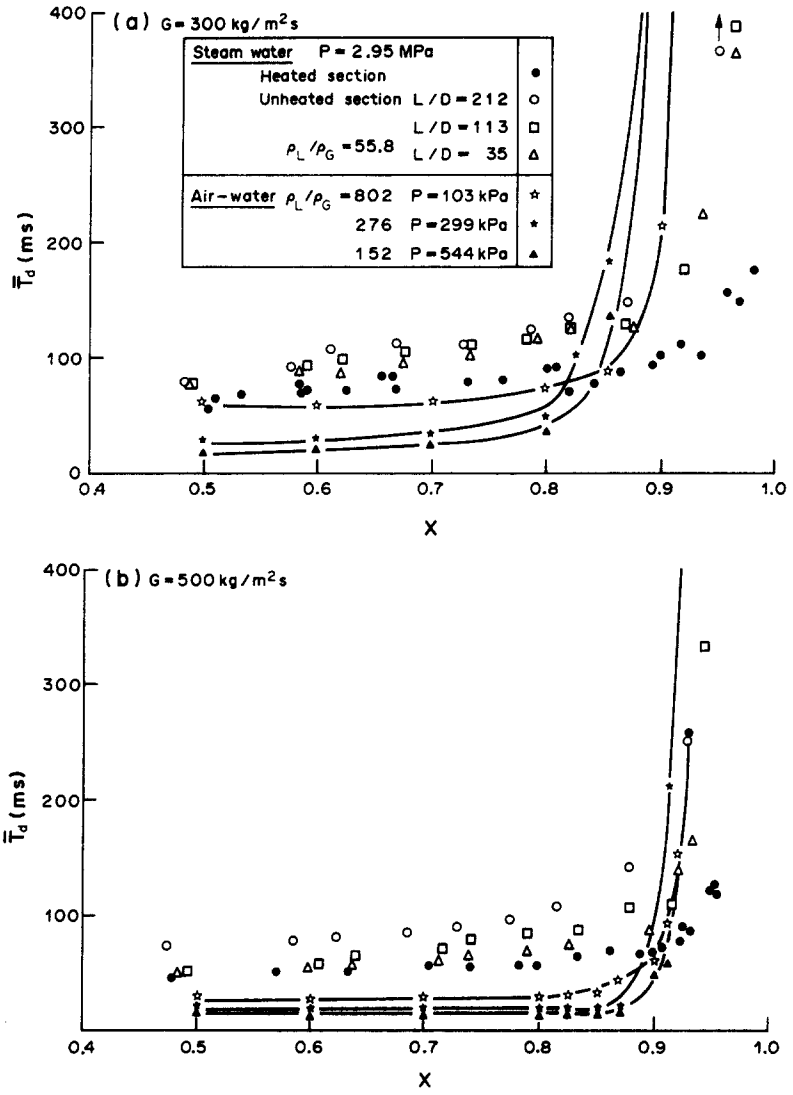

Figure 9. Mean time separation. Comparison of boiling flow data with adiabatic data.

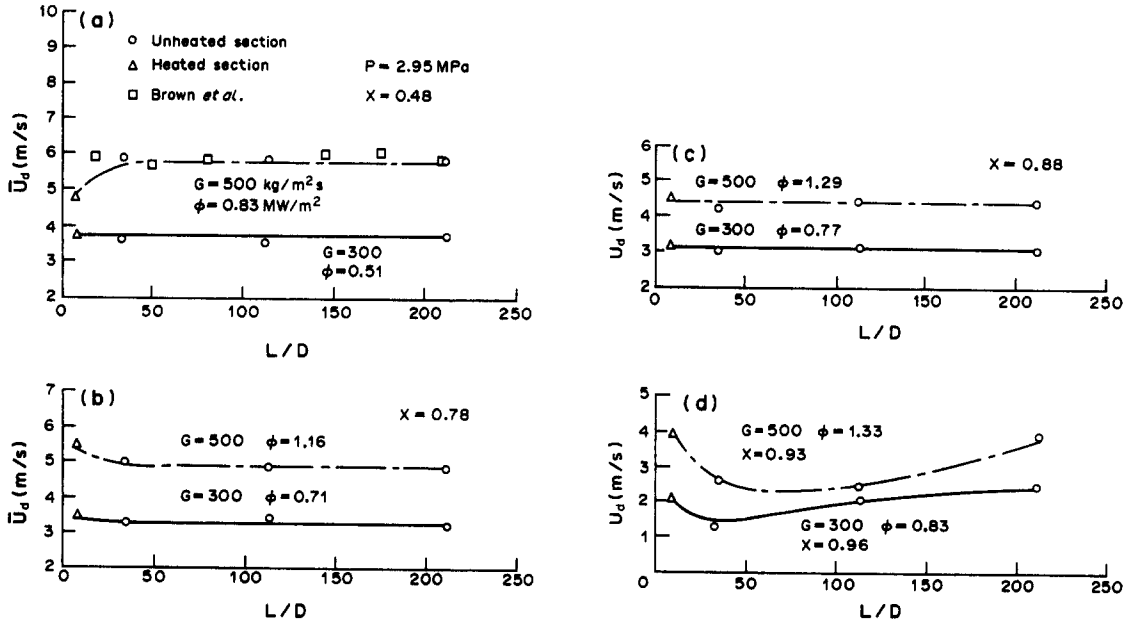

Figure 10. Variation of the propagation velocity along the unheated channel (steam–water system).

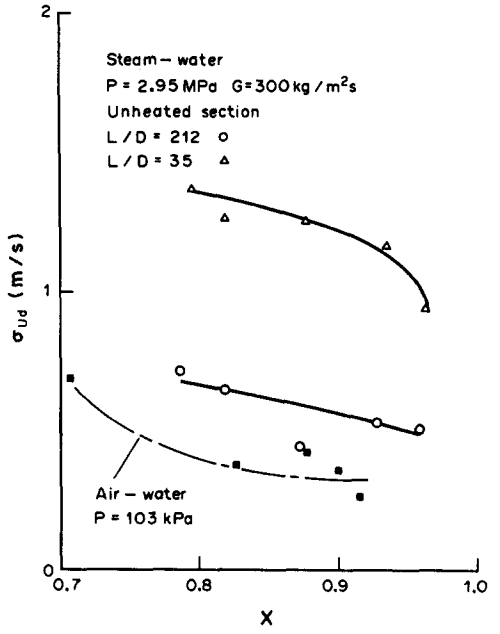

Figure 11. Variation of the standard deviation of the propagation velocity along the unheated channel (steam–water system).

mean propagation velocity in figure 10(d) is due to the inception of dryout in the neighborhood of the exit of the heated section. In this situation, the base film becomes extremely thin and may partly disappear, so the movement of the disturbance waves is retarded over the partially dried out channel wall. The increase in the propagation velocity is probably attributable to restoration of the base film due to the deposition of entrained droplets.

In contrast with the mean propagation velocity, the distinct effect of the B–D non-equilibrium was confirmed on the standard deviation of the propagation velocity, σ_{Ud}, as shown in figure 11. The standard deviation decreases along the unheated channel approaching that of the corresponding adiabatic air–water system.

Our data for the mean propagation velocity, $\bar{U}_d$, were correlated in terms of the interfacial shear stress, τ_i. For two-component two-phase flow such as in the air–water system, $\bar{U}_d$ is proportional to the friction velocity, v^*, in the range of $\pm 20\%$, as shown in figure 12; the friction velocity is defined for the liquid phase as $v^* = \sqrt{\tau_i/\rho_L}$, where ρ_L is the density of the liquid phase. On the other hand, for one-component two-phase flow, e.g. the steam–water and R113 boiling systems, $\bar{U}_d$ is

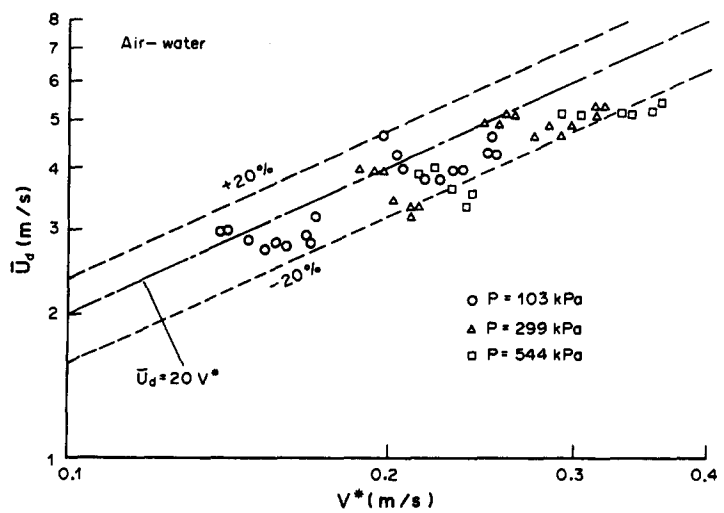

Figure 12. Correlation of the mean propagation velocity for the two-component system (air–water).

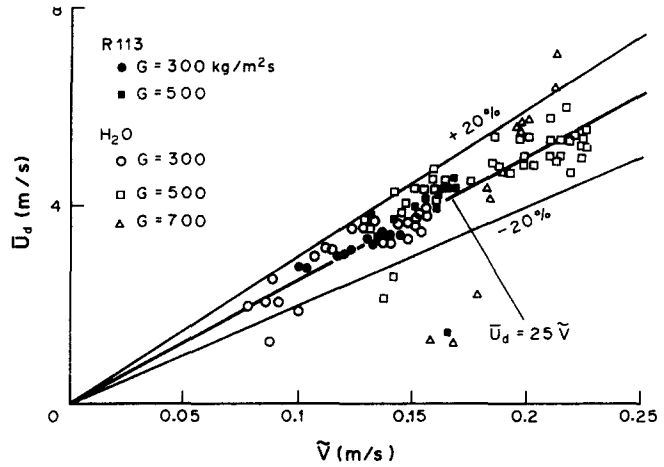

Figure 13. Correlation of the mean propagation velocity for the one-component system (steam–water and R113).

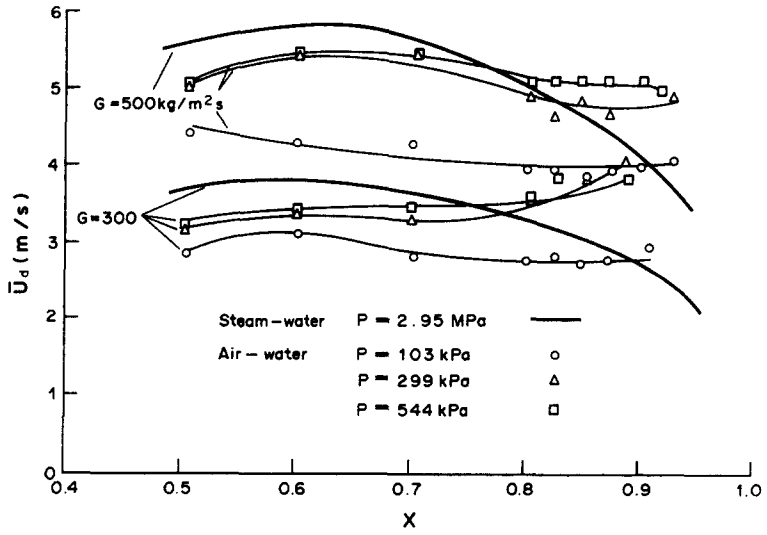

Figure 14. Mean propagation velocity. Comparison of boiling flow data with adiabatic data.

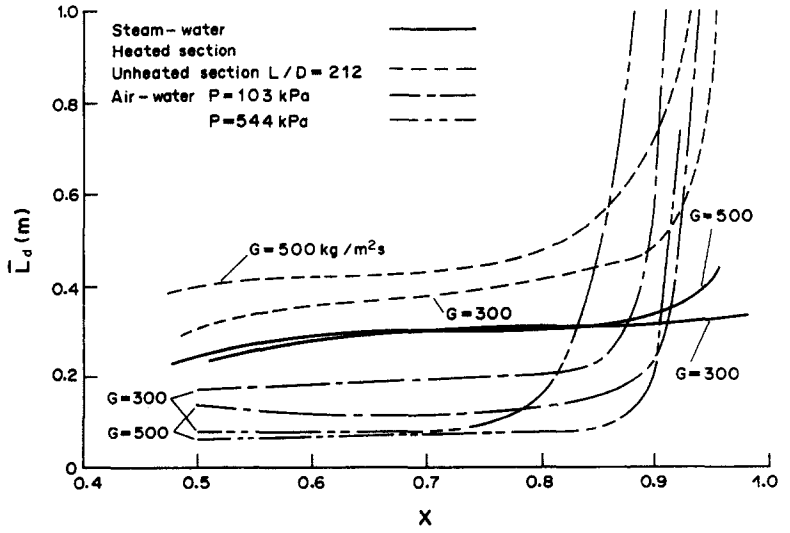

Figure 15. Mean space separation. Comparison of boiling flow data with adiabatic data.

proportional to $\tilde{v}$, the ratio of the interfacial shear stress to the mass flux, τ_i/G, as can be seen in figure 13. It is interesting that the same correlation is applicable to both these two systems irrespective of the differences in system pressure, tube diameter and working fluid. In both correlations, the interfacial shear stress, τ_i, is estimated using the Henstock & Hanratty (1970) correlation.

Figure 14 shows the mean propagation velocity, $\bar{U}_d$, vs quality, X, including the air–water system data for comparison. The difference between the two systems is remarkable in the high quality region and the air–water system data for higher pressures deviate farther from the steam–water system data.

3.4. Space separation of the disturbance waves

Figure 15 shows the mean value of the space separation, $\bar{L}_d$, between successive disturbance waves, defined as the product of the mean propagation velocity and the mean time separation. For the steam–water system, it remains constant and independent of quality in the heated channel, while it increases with quality in the unheated channel. The latter tendency also exists in the air–water system. This difference means that the hydrodynamic non-equilibrium affects the space separation.

4. SIMULATION OF THE B–D NON-EQUILIBRIUM WITH THE AIR–WATER SYSTEM

A simulation study of the B–D non-equilibrium with the air–water system was made on the rectangular test section in the test rig shown in figure 4. The flow pattern map of fully-developed flow is shown in figure 16. All experimental runs were conducted at the superficial air velocity, j_G, fixed to 10 m/s, for which the transition superficial water velocity from "ripples" to "disturbance waves without entrainment" is 6 mm/s, as seen from the figure (point '1'). The values of the superficial water velocity, j_{L1}, before liquid film sucking were 9 (point '1.5') and 12 mm/s (point '2'), both corresponding to the "disturbance waves without entrainment". The values of the superficial water velocity, j_{L2}, after sucking were 12, 9, 6, 4.5 and 3 mm/s; the last two values correspond to the "ripples" and denote points '0.75' and '0.5', respectively.

Figure 17 shows the variation of the thickness of the water film flow along the test channel for the runs with $j_{L1} = 12$ mm/s. The liquid film sucking was conducted between probes 2 and 3, generating B–D non-equilibrium there. At probe 3, the first conductance probe after the sucking

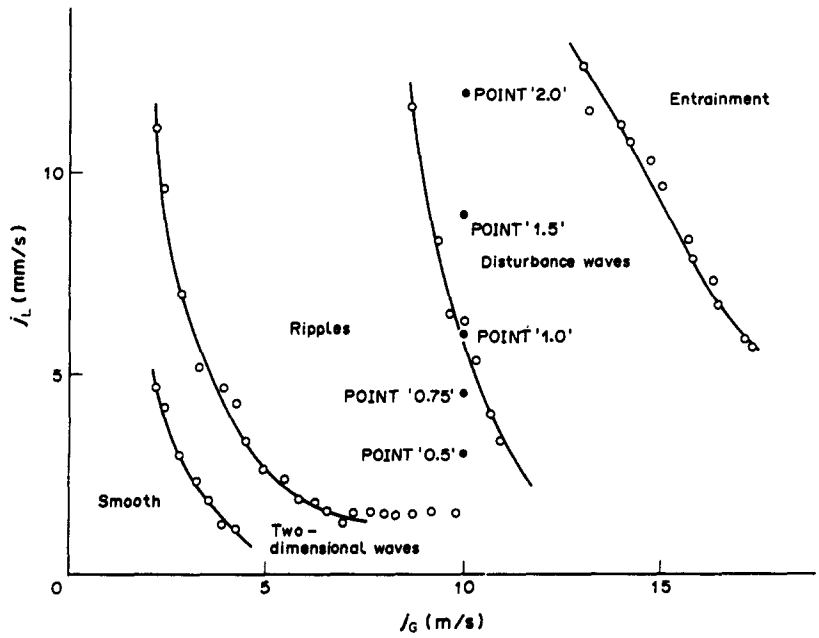

Figure 16. Flow pattern map of fully-developed shear flow.

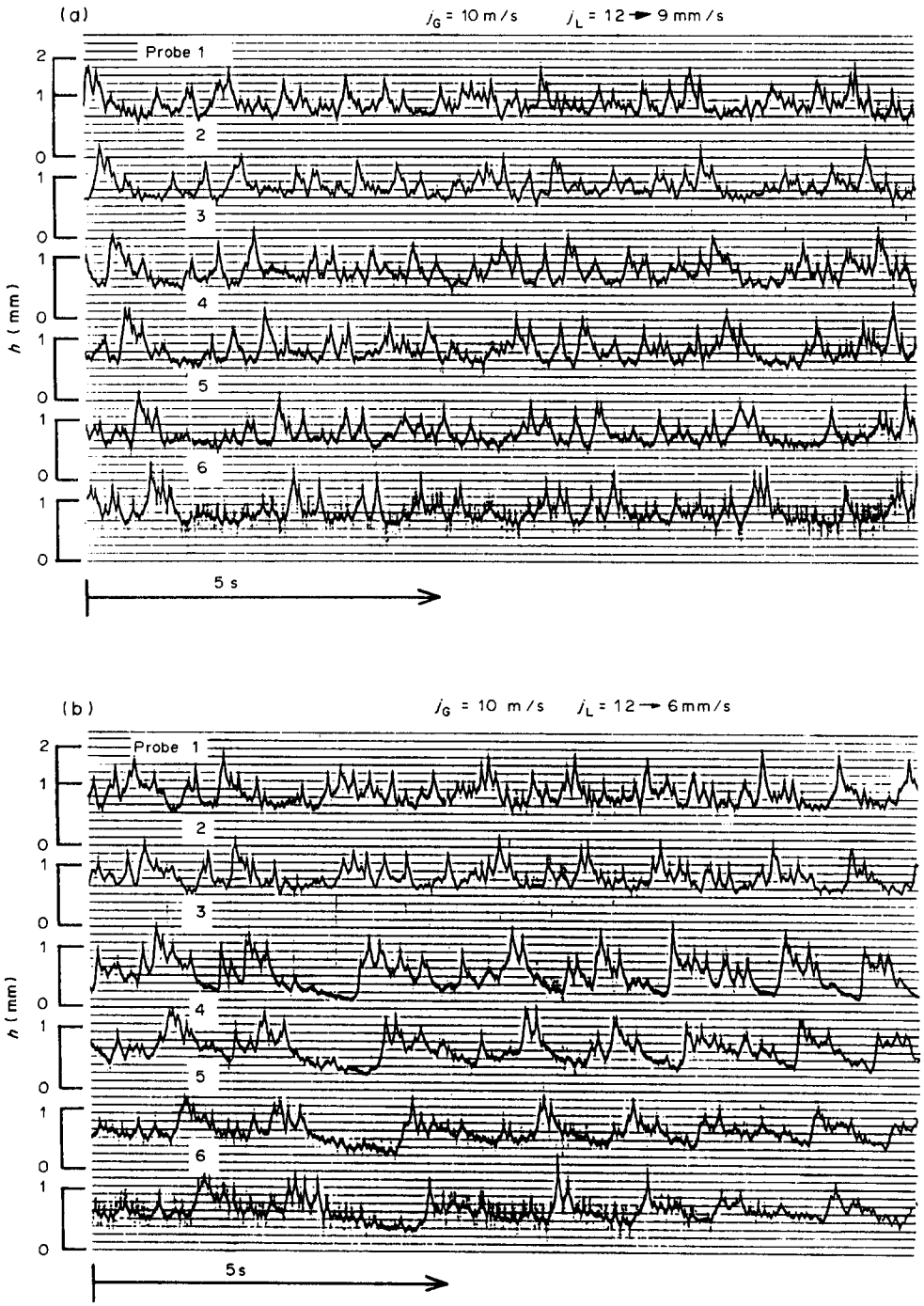

Figure 17—*continued opposite*

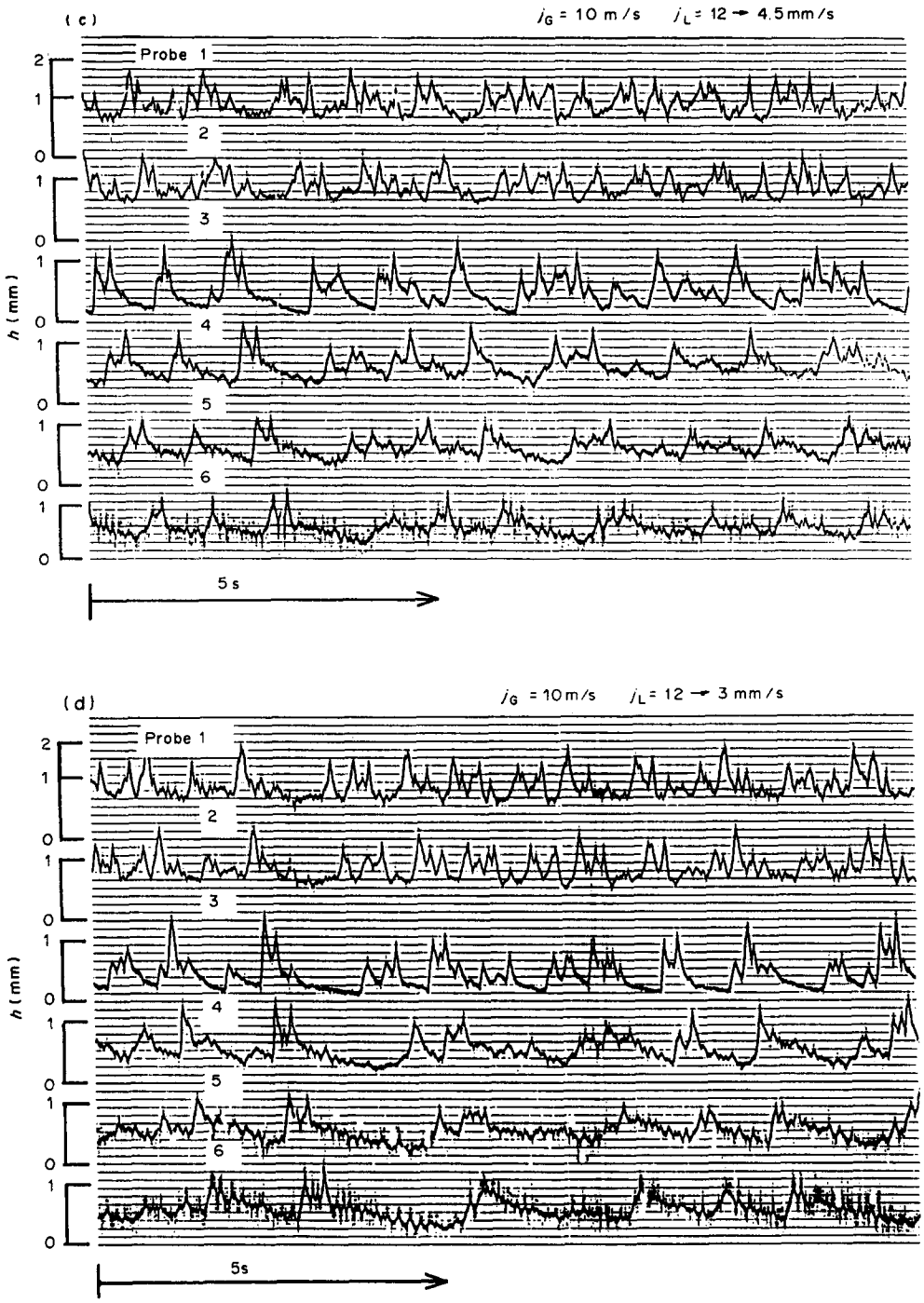

Figure 17. Variation of water film thickness: (a) $j_G = 10$ m/s, $j_L = 12$–9 mm/s (point '2.0' → point '1.5'); (b) $j_G = 10$ m/s, $j_L = 12$–6 mm/s (point '2.0' → point '1.0'); (c) $j_G = 10$ m/s, $j_L = 12$–4.5 mm/s (point '2.0' → point '0.75'); (d) $j_G = 10$ m/s, $j_L = 12$–3 mm/s (point '2.0' → point '0.5').

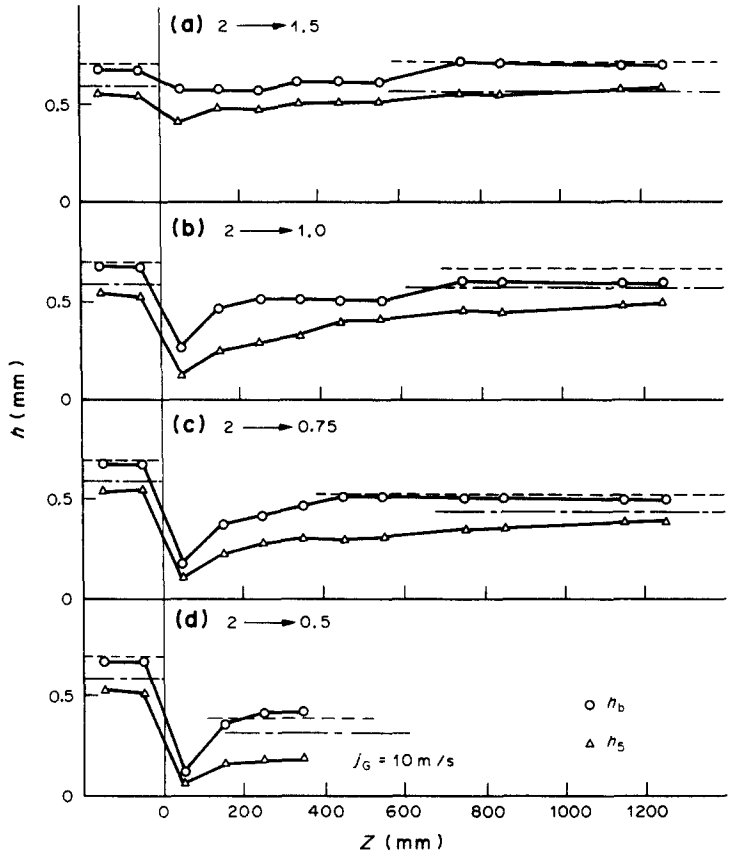

Figure 18. Recovery process of the film thickness fluctuation: (a) point '2.0' → point '1.5'; (b) point '2.0' → point '1.0'; (c) point '2.0' → point '0.75'; (d) point '2.0' → point '0.5'.

zone, a sudden decrease in the thickness of the base film was observed, while the height of the disturbance waves was virtually unchanged in all the runs. As the B–D equilibrium recovers, the height of the disturbance waves gradually decreases and the time separation increases along the channel. Smaller disturbance waves attenuate more rapidly than larger ones, and the latter survive or have longer lives. Under B–D non-equilibrium conditions, most of the disturbance waves acquire steeper front sides and longer tails at the rear than under B–D equilibrium or hydrodynamic equilibrium; the wave profiles are similar to those in boiling flow (see figure 6). This observation strongly supports our view about the nature of the non-equilibrium in boiling flow, in spite of the difference in the flow direction between the boiling flow and the air–water shear flow; there is a non-equilibrium distribution of liquid in the film flow between the base film and the disturbance waves, and the disturbance waves travel along the boiling channel feeding their excess liquid to the base film.

Figure 18 shows the recovery process of the base film along the test section, where the base film thickness, h_b, is defined as the thickness corresponding to the maximum of the probability density function of film thickness and the minimum film thickness, h_5, is that corresponding to a 5% cumulative distribution function. The --- and —·— lines in the figure represent the equilibrium values of h_b and h_5 for each run, respectively. Just after sucking, h_b and h_5 decrease suddenly and, then, gradually increase approaching the equilibrium value. The length required for recovery of the base film is about 800 mm when the "disturbance wave" regime is maintained after suction, and 200–500 mm when the regime changes to "ripples".

Figures 19 and 20 show the recovery process of the disturbance waves using $\bar{T}_d$ and $\bar{U}_d$, respectively. It is found that the mean value of the time separation increases over the whole length of the section where the conductance probes were mounted. While the mean value of the propagation velocity hardly varies, even after sucking. The increase in the time separation of the disturbance waves along the channel corresponds to the increase in the base film thickness shown

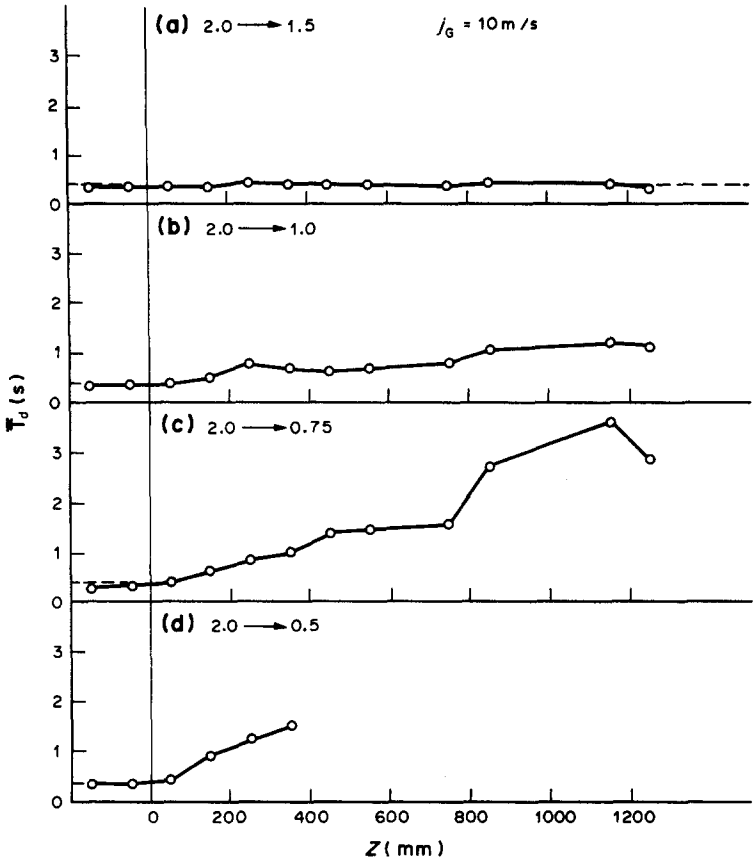

Figure 19. Recovery process of the mean time separation; (a) point '2.0' → point '1.5'; (b) point '2.0' → point '1.0'; (c) point '2.0' → point '0.75'; (d) point '2.0' → point '0.5'.

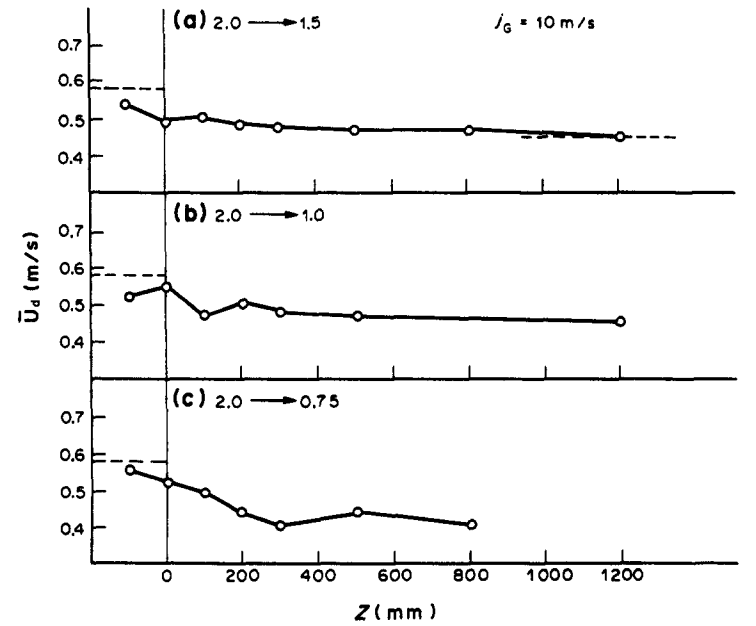

Figure 20. Recovery process of the mean propagation velocity: (a) point '2.0' → point '1.5'; (b) point '2.0' → point '1.0'; (c) point '2.0' → point '0.75'.

in figure 18, which shows that the base film recovers and the disturbance wave attenuates and, sometimes, disappears.

These observations support our proposal about the B–D hydrodynamic non-equilibrium and lead to the following interpretation of the behavior of disturbance waves in the boiling flow. The base film thickness is thinner and the mass of the disturbance waves is relatively more excessive in the boiling flow than in the hydrodynamic equilibrium flow. As a result, the disturbance waves tend to transfer the excessive liquid from their rear tail sides to the base film, thereby gradually attaining a symmetrical profile as they progress along the channel. From comparison with the data in the steam–water system stated above, it is suggested that the behavior of the disturbance waves just downstream of the sucking zone approximately simulates that in the boiling flow, and also that the recovery process from the non-equilibrium is very similar in both the air–water and steam–water systems: it is concluded that the liquid film sucking method with the air–water shear flow is qualitatively able to simulate the B–D non-equilibrium in the boiling flow and its recovery in the unheated section, in spite of the difference in the flow direction.

5. CONCLUSIONS

Through analysis of the experimental data for the liquid film thickness fluctuation in boiling flow and its change in an unheated channel obtained with a steam–water test rig, we have confirmed a new type of hydrodynamic non-equilibrium in the annular flow regime and identified it as the imbalance in the liquid distribution between the base film and the bodies of the disturbance waves ("B–D non-equilibrium"). Its existence in boiling flow was also confirmed by the simulation of B–D non-equilibrium with air–water shear flow, which threw light on the inherent behavior of the disturbance waves in boiling two-phase flow.

However, even in the flow which considered to be a fully-developed adiabatic one, some differences were still observed in the mean propagation velocity and the wave profile when the steam–water and air–water data were compared. From analysis of the air–water data under different pressures, it is unlikely that effect of the gas–liquid density ratio is one of the possible causes of this difference.

Acknowledgements—The authors wish to express their gratitude to Associate Professor M. Kaji (Osaka University) for his valuable criticisms and discussions, and to Messrs T. Matta, A. Kanbara and H. Mibu for their help in conducting the experiments.

REFERENCES

BROWN, D. J., JENSEN, A. & WHALLEY, P. B. 1975 Non-equilibrium effects in heated and unheated annular two-phase flow. ASME Paper 75-WA/HT/7, pp. 1–7.

HENSTOCK, W. H. & HANRATTY, T. J. 1970 The interfacial drag and the height of the wall layer in annular flows. *AIChE Jl* **26,** 990–999.

KAWATA, S. & MINAMI, S. 1984 Adaptive smoothing of spectropic data by linear mean square estimation. *Appl. Spectrosc.* **38,** 49–58.

NAKANISHI, S., YAMAUCHI, S., ISHIGAI, S. & KOTANI, H. 1982 Wall temperature fluctuation of the evaporating tube at the dryout region. *Proc. 7th Int. Heat Transfer Conf.* **4,** 315–320.

NAKANISHI, S., KAJI, M., YAMAUCHI, S., KAZUOKA, Y. & SAWAI, T. 1985 Behavior of disturbance waves in the dryout region. *PhysicoChem. Hydrodynam.* **6,** 157–164.

TONG, L. S. & HEWITT, G. F. 1972 Overall viewpoint of flow-boiling CHF mechanisms. ASME Paper 72-HT-54.